PHYSICAL REVIEW D **79,** 103507 (2009)

Avoiding the blue spectrum and the fine-tuning of initial conditions in hybrid inflation

Sébastien Clesse[1,2,*] and Jonathan Rocher[1,†]

[1]*Service de Physique Théorique, CP225, Université Libre de Bruxelles, Bld du Triomphe, 1050 Brussels, Belgium*
[2]*Center for Particle Physics and Phenomenology, Louvain University, 2 chemin du cyclotron, 1348 Louvain-la-Neuve, Belgium*
(Received 29 September 2008; published 7 May 2009)

Hybrid inflation faces two well-known problems: the blue spectrum of the nonsupersymmetric version of the model and the fine-tuning of the initial conditions of the fields leading to sufficient inflation to account for the standard cosmological problems. They are investigated by studying the exact two-fields dynamics instead of assuming slow-roll. When the field values are restricted to be less than the reduced Planck mass, a non-negligible part of the initial condition space (around 15% depending on potential parameters) leads to successful inflation. Most of it is located outside the usual inflationary valley and organized in continuous patterns instead of being isolated as previously found. Their existence is explained and their properties are studied. This shows that no excessive fine-tuning is required for successful hybrid inflation. Moreover, by extending the initial condition space to Planckian-like or super-Planckian values, inflation becomes generically sufficiently long and can produce a red-tilted scalar power spectrum due to slow-roll violations. The robustness of these properties is confirmed by conducting our analysis on three other models of hybrid-type inflation in various framework: ''smooth'' and ''shifted'' inflation in SUSY and SUGRA, and ''radion assisted'' gauge inflation. A high percentage of successful inflation for smooth hybrid inflation (up to 80%) is observed.

DOI: 10.1103/PhysRevD.79.103507 PACS numbers: 98.80.Cq

I. INTRODUCTION

For almost a decade, the cosmic microwave background data have supported a cosmological concordance model, in which inflation [1–5], an early phase of accelerated expansion, is the favored explanation for the origin of the primordial fluctuations.[1] For more than 25 years, many models of inflation have been proposed, from toy models to more realistic models based on various high energy physics frameworks [4,9–11]. The incoming flow of cosmological data has however started to discriminate among the models. In particular, the last release of the WMAP 5-years data [12] favored a red-tilted scalar power spectrum.

If some single-field models are still able to reproduce the current data, the presence of multiple scalar fields in all the high energy physics frameworks proposed today (Higgs fields in grand unified theories, superpartners in supersymmetry, moduli in string theory) makes it hard to imagine that the inflaton field is not coupled to any other scalars. The simplest (and yet motivated) known example of multi-field inflation is the hybrid one. The original hybrid model of inflation, proposed in [13,14], had been introduced as an alternative way to end inflation and could be realized for sub-Planckian field values unlike chaotic models. The key idea is to couple the inflaton field to a Higgs-type waterfall field which ends inflation by acquiring a nonvanishing vacuum expectation value (vev). This model could be considered as realistic if employing a Higgs field and an extra singlet of some minimal extension of the standard model of particle physics. It also represents a toy model for many multifield models of inflation in other frameworks. Indeed, hybrid(-type) models of inflation have been embedded in almost all high energy frameworks: in (extended) supersymmetry and supergravity [15–18], in grand unified theories [19,20], or various extra-dimensional theories [21–24].

When confronting the original hybrid inflation to the CMB data, it is however well-known [9] that the power spectrum tilt is blue which is now disfavored. This is only valid when slow-roll is assumed and when the vacuum energy density dominates the potential since in the other case, the potential becomes equivalent to a chaotic model. In this paper, we illustrate these properties and study the predictions for the spectral index of the model using the exact field dynamics. We find a new way to generate a red-tilted spectrum due to nontrivial effects of the violation of slow-roll, give the two possible conditions on the parameters of the potential to generate a red spectrum of perturbations and discuss the field values that these conditions require.

Several fundamental questions about initial conditions for inflation are still open (see for example [25–31]). In this paper, we will not address the important problem of spatial homogeneity of the fields [25] and we will assume that the field values do not enter the self-reproducing inflationary regime [28]. Even when restricting to the classical approxi-

*seclesse@ulb.ac.be
†jrocher@ulb.ac.be

[1]Note however that some alternatives exist such as string gas cosmology [6] or bouncing universe models [7,8].

mation, the existence of a fine-tuning on the initial values of the fields was found, for hybrid inflation [29–31]. (An opposite conclusion has been obtained [32] for the smooth hybrid inflation model. We will comment on this model at Sec. III). The space of initial conditions is described by regions in the plane (ϕ_i, ψ_i), where ϕ_i and ψ_i denote the initial values of the inflaton and the waterfall field, respectively. By fine-tuning of the initial conditions, one means that the regions leading to sufficient (60 e-folds or more) inflation have been found to be composed [29,31] of an extremely thin band around $\psi_i = 0$ and a few apparently random points in the rest of the plane. Uncertainties remain on whether these points are of null measure [31] or not [29]. The thin band is also considered as fine-tuned because ψ_i has to be so close to 0 that any quantum fluctuations would shift its value outside the successful region [29]. This would be an important problem for hybrid-type inflation because it means that these models would not easily be the natural outcome of some preinflationary era (see however [33]).

Several papers have proposed some solutions to the fine-tuning problems. It has been proposed to replicate many times identically the inflaton sector [31], even though no motivations have been proposed for this replication. A similar idea had been employed to construct the N-flation model [34] but the replication in this context is not more natural [35]. It has also been proposed [31,36] to embed hybrid inflation into a brane description. The induced modifications to the Friedmann-Lemaître equations provide additional friction in the evolution of scalar fields. Thus slow-rolling is favored and more of the initial condition space gives rise to successful inflation. This friction can also be efficiently played by dissipative effects [37], when couplings between the inflaton and the waterfall field with a bath of other fields are assumed. Finally, it has been proposed [38] to solve this problem by accepting a short ($N \sim 10$) phase of hybrid inflation and implementing a second one responsible for the generation of the primordial fluctuations, thus solving the horizon problem.

However, to our knowledge, little has been proposed to explain the properties of the (un-)successful space of initial conditions: discreteness, subdominance, size and limits. In this paper, we first show that super-Planckian initial conditions always give rise to a sufficiently long phase of hybrid inflation and can produce a red-tilted power spectrum without the need of any fine-tuning. We provide a detailed analysis of the properties of the initial condition space, explain why parts of this space were thought to be discrete, and what are the field trajectories leading to these apparently isolated points. In particular, we show that they can be viewed as the ''anamorphosis'' (that is a deformed image) of the thin successful band. We also give the area of successful initial conditions in the plane (ϕ_i, ψ_i). Even when restricting the fields to sub-Planckian values, we find around 15% of successful initial conditions and we discuss the effect of varying the different parameters of the potential. When going to super-Planckian values, we confirm that this ratio tends to 100%.

To prove the robustness of these results, we explore the space of initial conditions for three other hybrid-type models: the supersymmetric and supergravity smooth [39–41] and shifted [42,43] models, as well as the ''radion assisted'' gauge inflation [24]. The first two models are direct extensions of the F-term hybrid inflation [17] and are motivated by the fact that their inflationary valley is shifted away from $\psi = 0$, so that any harmful topological defects formed during the symmetry breaking induced by ψ would be diluted away. The last model is based on a hybrid-type potential even though constructed in 5D. Its main motivation resides in the fact, that by construction, the form of the potential is controlled (and thus protected) by gauge symmetries.

Before going any further, let us discuss the physical motivations of enlarging the space of initial conditions to super-Planckian values. Even though this possibility has been moderately studied in [30], most previous works [29,31] restricted their analysis to initial values of the fields under the Planck mass. For nonsupersymmetric four-dimensional theories, it was proposed in [4] that quantum gravity corrections are controlled as long as the energy density and the effective masses are sub-Planckian. In this case, effective field theories can be an appropriate framework to describe fields of Planckian-like amplitude. More recently, several models such as natural inflation [44], or gauge inflation [45–47] also allow fields to be super-Plankian. For example, in gauge inflation, the inflaton field is part of a gauge field and thus the form of the potential is protected by gauge symmetries, leaving nonrenormalizable corrections highly constrained.

Let us turn to supersymmetric frameworks. Since uncontrolled nonrenormalizable corrections to the superpotential and the Kähler potential appear, super-Planckian fields are inevitably problematic for models constructed in the context of supersymmetry (SUSY) or supergravity (SUGRA). Global SUSY is only valid as long as all fields have an amplitude much smaller than[2] M_{pl}. When closer to the reduced Planck mass (but still below), SUGRA corrections are important and supergravity is the correct framework to describe the model. Above M_{pl}, the nonrenormalizable corrections become dominant: the nonrenormalizability of SUGRA prevents us from using it and a UV-complete theory is then necessary [48]. Finding and describing inflaton fields with Planckian displacements in string theories is, however, possible in certain sectors of string theories, though not always stable and their potential is not easily flat [48,49]. Several models of inflation constructed within string theories have been proposed (see for

[2]Throughout this paper, we will denote the Planck mass by $m_{pl} \equiv G^{-1/2} \simeq 1.2 \times 10^{19}$ GeV and the reduced Planck mass by $M_{pl} \equiv (8\pi G)^{-1/2}$.

e.g. [11,48,50,51] and refs therein) and some of them have a low-energy effective description that mimics hybrid inflation [10,21,22]. *These examples motivated us to assume that the effective inflationary potentials studied in this paper can also originate from frameworks in which it is safe to consider super-Planckian fields.* As a conclusion, we have chosen to study them both in the sub-Planckian and super-Planckian field regimes. However, we will always restrict ourselves to sub-Planckian energy densities.

The rest of the paper is organized as follows. In the Sec. II, we extensively study the original hybrid inflation model [13]. In particular, we discuss the validity of the one-field slow-roll approximation and show that violation of slow-roll conditions can strongly modify the dynamics. Using exact numerical methods, applied on the two-field potential, we provide a complete analysis of the space of initial conditions and revisit the above-mentioned fine-tuning problem. In Sec. III, we test the robustness of our results on the three other models: SUSY/SUGRA smooth hybrid inflation, SUSY/SUGRA shifted hybrid inflation and radion-inflation. Our conclusions are drawn in Sec. IV and some open questions are developed.

II. ORIGINAL HYBRID MODEL

Proposed in [13,14], the model is based on the potential

$$V(\phi, \psi) = \frac{1}{2}m^2\phi^2 + \frac{\lambda}{4}(\psi^2 - M^2)^2 + \frac{\lambda'}{2}\phi^2\psi^2, \quad (1)$$

where ϕ is the inflaton and ψ is the Higgs-type field. λ and λ' are two positive coupling constants, m and M are two mass parameters. It is the most general form (omitting a quartic term $\lambda''\phi^4$) of renormalizable potential verifying the symmetries $\psi \leftrightarrow -\psi$ and $\phi \leftrightarrow -\phi$. In the general case, inflation is mostly assumed to be realized in the false-vacuum along the $\psi = 0$ valley and ends with a tachyonic instability for the Higgs-type field. The critical point of instability below which the potential develops nonvanishing minima is

$$\phi_c = M\sqrt{\frac{\lambda}{\lambda'}}. \quad (2)$$

The system then evolves toward its true minimum at $V = 0$, $\langle\phi\rangle = 0$, and $\langle\psi\rangle = \pm M$, where throughout the paper, $\langle . \rangle$ denotes the vacuum expectation value (vev) of a field.

In this section, we will first restrict ourselves to the effective one-field approach to reanalyze the predictions of the spectral index for the generated power spectrum. This will be done solving numerically the exact field equations of motion rather than assuming slow-roll. Then, we will move one the full two-field dynamics and study the initial conditions that lead to sufficiently long inflation.

A. Effective one-field potential

To study the inflationary phase along the valley $\psi = 0$, it is common usage to restrict the potential of Eq. (1) to a one-dimensional effective potential of the form

$$V(\phi) = \Lambda^4\left[1 + \left(\frac{\phi}{\mu}\right)^2\right], \quad (3)$$

with

$$\mu \equiv \sqrt{\frac{\lambda}{2}}\frac{M^2}{m}, \qquad \Lambda \equiv \lambda^{1/4}M/\sqrt{2}. \quad (4)$$

The Friedmann-Lemaître equations and the Klein-Gordon equation in an expanding universe for this scalar field read

$$\begin{aligned} H^2 &= \frac{8\pi}{3m_{\rm pl}^2}\left[\frac{1}{2}\dot{\phi}^2 + V(\phi)\right], \\ \frac{\ddot{a}}{a} &= \frac{8\pi}{3m_{\rm pl}^2}[-\dot{\phi}^2 + V(\phi)], \end{aligned} \quad (5)$$

$$\ddot{\phi} + 3H\dot{\phi} + \frac{dV}{d\phi} = 0, \quad (6)$$

where a is the scale factor, H the Hubble parameter, and the dot denotes a derivative with respect to cosmic time. Inflation is realized starting at high field values, the field rolling down toward 0. To mimic the two-field dynamics, in this effective model, it is necessary to define an effective critical value $\phi_c > 0$ at which inflation ends.

The well-known slow-roll approximation consists in neglecting the second derivative of the field in Eq. (6) and the kinetic terms compared to the potential in Eq. (5). Using the Hubble-flow parameters [52,53]

$$\epsilon_0 \equiv H, \qquad \epsilon_{n+1} \equiv \frac{d\ln\epsilon_n}{dN}, \quad (7)$$

inflation occurs for $\epsilon_1 = -\dot{H}/H^2 < 1$ and slow-roll conditions are satisfied when, for all $n \geq 1$, $|\epsilon_n| \ll 1$. For the effective hybrid potential, an analytical expression of the first and second Hubble-flow parameter is easily derived in the slow-roll approximation,

$$\begin{aligned} \epsilon_1(\phi) &= \frac{1}{4\pi}\left(\frac{m_{\rm pl}}{\mu}\right)^2\frac{(\phi/\mu)^2}{[1 + (\phi/\mu)^2]^2}, \\ \epsilon_2(\phi) &= \frac{1}{2\pi}\left(\frac{m_{\rm pl}}{\mu}\right)^2\frac{(\phi/\mu)^2 - 1}{[1 + (\phi/\mu)^2]^2}. \end{aligned} \quad (8)$$

It is clear from these expressions that the slow-roll conditions are satisfied for large field values. As illustrated in Fig. 1, Eq. (8) suggests that two phases of inflation can take place [54]. A first phase at large values of the field, and a

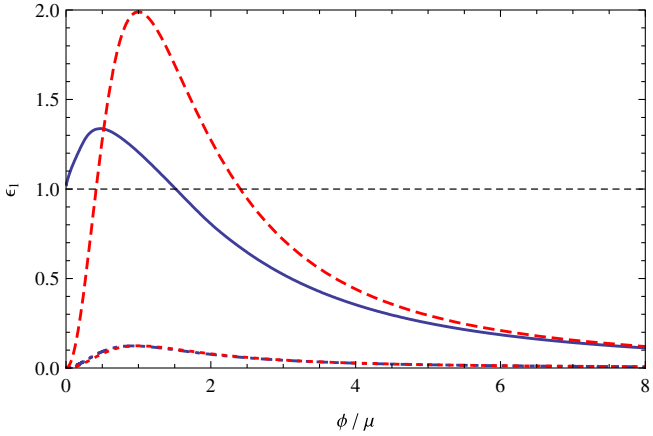

FIG. 1 (color online). First Hubble-flow parameter ϵ_1, function of the inflaton field, during its evolution started in the large field phase, in the slow-roll approximation (red dashed and dotted lines) and from the exact dynamics (blue solid and dot-dashed lines). The curves correspond to $\mu = 0.1 m_{\rm pl}$ (two top curves), $\mu = 0.4 m_{\rm pl}$ (two bottom curves, quasisuperimposed). For each value of μ, we observe two phases of evolution at large field and at small field (compared to $\phi_{\rm max}$).

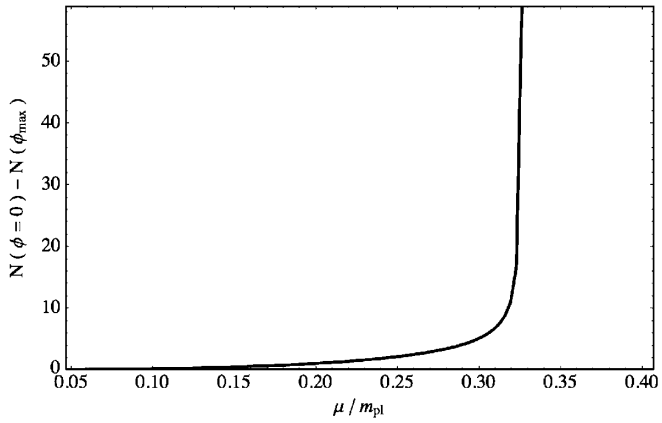

FIG. 2. Number of e-folds created between $\phi_{\rm max}$ and $\phi = 0$ as a function of μ, when slow-roll is not assumed. There exist a critical value of the parameter μ under which a marginal number of e-folds is generated in the second phase of evolution. Above the critical value of μ, the number of e-folds created in the second phase of inflation diverges showing the efficiency of the second phase of inflation when it exists.

second phase at small values. These phases are separated by a maximum of $\epsilon_1(\phi)$, reached at $\phi_{\rm max}$, and at which $\epsilon_2(\phi)$ changes its sign. In the slow-roll approximation $\phi_{\rm max} = \mu$. However, around $\phi_{\rm max}$, and for sufficiently small values of μ, slow-roll conditions can be violated, as it is illustrated by the dashed line in Fig. 1. Thus a resolution of the exact equations of motion for the fields is required to study the influence of the transition period on the dynamics of inflation.

1. Exact field dynamics

The dynamics of the one-field effective hybrid inflation, without assuming slow-roll, is described by Eqs. (5) and (6): they have been integrated numerically. The parameter ϵ_1 has been computed exactly and is represented as a function of the inflaton field in Fig. 1 and compared to the analytical slow-roll expressions of Eq. (8).

The exact integration confirms the existence of the two regimes before and after the maximum of ϵ_1, at which the slow-roll conditions can be violated and inflation can even be interrupted (when $\epsilon_1 \geq 1$) depending on the value of the parameter μ. But there are two important novelties. Firstly, $\phi_{\rm max}$ is displaced toward *smaller* values in the exact treatment compared to its slow-roll value μ. Secondly, in the slow-roll approximation, after the peak, $\epsilon_1(\phi)$ decreases and vanishes for vanishing field. One may think that inflation always takes place for $\phi < \phi_{\rm max}$. However, exact numerical results show that this conclusion is erroneous: ϵ_1 does not necessarily become negligible when the field vanishes (see the plain blue curve). As a consequence, *inflation does not necessarily produce the last* 60 *e-folds in the small field regime* ($\phi < \phi_{\rm max}$).

From Fig. 1, it is clear that the presence or not of small field phase of inflation depend on the parameter μ (difference between the dashed and plain curves). In order to measure the efficiency/existence of this second phase of inflation, we have plotted in Fig. 2 the number of e-folds created between $\phi_{\rm max}$ and $\phi = 0$ as a function of μ. This shows that there exists a critical value

$$\mu_{\rm crit} \simeq 0.32 m_{\rm pl}, \tag{9}$$

under which the number of e-folds generated after $\phi_{\rm max}$ is reached is marginal. In this case, the period of inflation where the observable modes become super-Hubble will always take place in the large field phase ($\phi > \phi_{\rm max}$) provided $\phi_{\rm i} > \phi_{\rm max}$. In this case, the potential of hybrid inflation leads to a chaoticlike inflation, independently of the way inflation ends. This has important consequences for the generated spectral index.

2. Scalar spectral index

At first order in slow-roll parameters, the spectral index of the scalar power spectrum $\mathcal{P}_\zeta$ can be expressed as [52,55]

$$n_{\rm s} - 1 \equiv \frac{d\mathcal{P}_\zeta}{d\ln k}\bigg|_{k=k_*} = -2\epsilon_{1*} - \epsilon_{2*}. \tag{10}$$

A star means that the quantity is evaluated at Hubble crossing $aH = k_*$, k_* being a pivot scale in the range of observable modes.

Recent experimental results from WMAP 5-years [12] have a best fit at $n_{\rm s} \simeq 0.96$ and disfavor a value of the scalar spectral index greater than unity at almost 95% confidence level (CL). From this observation, hybrid models have recently been considered as disfavored. Indeed, in the

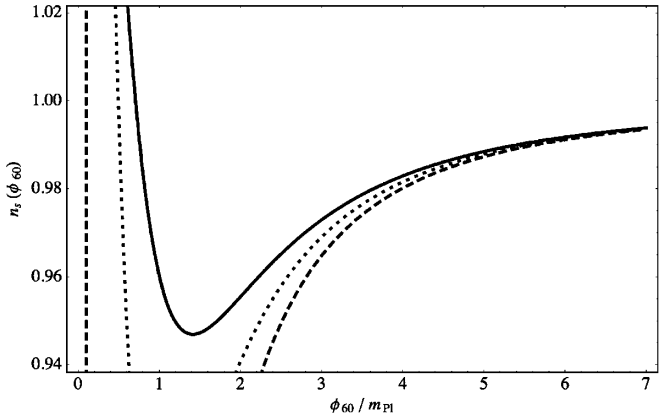

FIG. 3. Spectral index n_s of the power spectrum as a function of ϕ_{60}, the value of the field 60 e-folds before the end of inflation. This has been computed for the effective hybrid potential for $\mu = m_{\rm pl}$ (full line), $\mu = 0.7m_{\rm pl}$ (dotted line) and $\mu = 0.14m_{\rm pl}$ (dashed line), in the slow-roll approximation. One can see that almost any value of the spectral index can be accommodated within hybrid inflation.

slow-rolling effective one-field model, as shown at the previous section, the last 60 e-folds of inflation are realized in the small field phase characterized by a negative ϵ_2 and a negligibly small ϵ_1 which induces necessarily a blue spectrum.

However, there exist two mechanisms to produce a red spectrum within the standard hybrid inflation model along the valley $\psi = 0$. There are two ways of forcing the small field inflation phase not to take place, either by instability or by violation of the slow-roll condition. In both case, the consequence is that the spectral index generated is below 1 as represented in Fig. 3. Note that almost any values of the spectral index can be actually accommodated by the model, including the best fit for WMAP5 data.

When the critical point of instability is in the large field phase.—The simplest way to obtain a red spectrum is to destabilize inflation with the waterfall field at some stage during the large field phase or at most at the peak, $\phi_c \geq \phi_{\rm max}$, independently of μ. This had been noticed in the past [14,56], though not often emphasized. For $\phi \gg \phi_{\rm max}$, the inflaton potential is of the form $V \simeq m^2\phi^2/2$ for which $n_s < 1$. Since in the exact treatment $\phi_{\rm max} < \mu$ is shifted to smaller values, a sufficient condition to have $n_s < 1$ reads

$$\frac{m}{M} > \sqrt{\frac{\lambda'}{2}}. \tag{11}$$

This property still holds when violations of slow-roll are taken into account.

We would like to emphasize that the value of the inflaton 60 e-folds before the end of inflation, denoted ϕ_{60}, is necessarily super-Planckian if inflation takes place in the large field regime, independently of μ. If $\mu \geq \mu_{\rm crit}$, the slow-roll approximations can be used and with $\phi_{\rm end} = \phi_c = \phi_{\rm max} = \mu$, it is well-known [14] that the minimum value of ϕ_{60} is given by

$$\frac{2\pi\mu^2}{m_{\rm pl}^2}\left[2\ln\left(\frac{\phi_{60}}{\mu}\right) + \left(\frac{\phi_{60}}{\mu}\right)^2 - 1\right] = N_{\rm succ} = 60, \tag{12}$$

which is always around $3m_{\rm pl}$ or greater. If $\mu \leq \mu_{\rm crit}$, solving numerically the exact field dynamics is required, and we also found that $\phi_{60} \gtrsim 3m_{\rm pl}$.

When the second phase never takes place.—Assuming that the initial value is in the large field phase $\phi_i > \phi_{\rm max}$, if $\mu \lesssim \mu_{\rm crit}$, then the small field phase of inflation can never take place. This is a new way to generate a red spectrum independently of the critical value ϕ_c. Indeed, an excessive velocity of the field around $\phi_{\rm max}$ induces a violation of the (slow-roll) inflation condition (see plain line of Fig. 1). Thus ϕ_{60} necessarily lies in the large field regime and the spectrum is red, independently of the critical value ϕ_c. Notice however that even for $\mu \leq \mu_{\rm crit}$, one could still start an inflationary period with $\phi_i \ll \phi_{\rm max}$ leading to a blue-tilted power spectrum. Violation of slow-roll only prevents this period to occurs after any large field phase. In this case also, this requires a large initial value of the inflaton, and a realization of hybrid inflation in a regime away from the usual limit $\phi \ll \mu$. This conclusion might reduce the appeal of the model.

B. Exact two-field dynamics and initial conditions

We now turn to the two-field potential given in Eq. (1) to study the field dynamics without restricting to the $\psi = 0$ valley. In previous works, Tetradis [29], Lazarides & Vlachos [30] and more recently Mendes & Liddle [31] studied the space of initial conditions of the fields leading to successful/unsuccessful inflation for hybrid inflation. They found that the successful regions for sub-Planckian initial values are made of a very narrow band along the $\psi = 0$ axis (motivating the one-field approach), together with some scattered points in the unsuccessful region, which seemed randomly distributed. In this section, we explore a larger space of initial conditions and extend previous studies to super-Planckian initial values. We show that three different classes of successful trajectories in field space can be defined, one of them explaining the origin and the properties of the previously found isolated points. Finally, we quantify the amount of fine-tuning of the model by computing the ratio of successful/unsuccessful area and study the effect of varying the parameters of the potential on our results.

1. Exact two-field dynamics

For two homogeneous scalar fields ϕ and ψ, the Friedmann-Lemaître equations take the form

$$H^2 = \frac{8\pi}{3m_{\rm pl}^2}\left[\frac{1}{2}(\dot\phi^2 + \dot\psi^2) + V(\phi, \psi)\right],$$
$$\frac{\ddot a}{a} = \frac{8\pi}{3m_{\rm pl}^2}[-\dot\phi^2 - \dot\psi^2 + V(\phi, \psi)], \quad (13)$$

while the equations of Klein-Gordon for these scalar fields read

$$\ddot\phi + 3H\dot\phi + \frac{\partial V(\phi, \psi)}{\partial\phi} = 0,$$
$$\ddot\psi + 3H\dot\psi + \frac{\partial V(\phi, \psi)}{\partial\psi} = 0. \quad (14)$$

For the numerical integration, instead of using the scale factor and its time derivative as integration variables, it is more convenient to use the number of e-folds realized from the beginning of inflation[3] $N(t) = \ln[a(t)/a_{\rm i}]$ and its first derivative—the Hubble parameter.

2. Classical dynamics and stochastic effects

Considering large values for the fields can induce stochastic (quantum) effects to affect the field dynamics, described in this paper as purely classical [57,58]. Since we also consider super-Planckian field values, it is important to check that for such values, the dynamics is still dominated by the classical motion. The stochastic effects in the full two-field potential have not yet been studied but the stochastic effects should be very limited. Indeed, the dynamics that is found is fast-rolling at the beginning, during which the classical motion will clearly dominate and then slow-roll in the inflationary valley. When slow-roll is realized, it is possible to evaluate at what field values the stochastic effects become relevant by comparing the classical field fluctuations and the quantum field fluctuations, during a Hubble time. In the valley $\psi = 0$, we obtain

$$\frac{H}{2\pi} \gtrsim \frac{M_{\rm pl}^2 V'}{V} \Leftrightarrow \frac{\phi}{m_{\rm pl}^2} \gtrsim \frac{1}{2}\sqrt{\frac{3}{4\pi}}\frac{m_{\rm pl}}{m}. \quad (15)$$

Since the values of m used in this paper are well below the Planck scale, the stochastic effects are expected to be negligible even for field values of a few Planck scale [58].

3. Exploration of the space of initial conditions

Let us now study the space of initial values [i.e. the $(\phi_{\rm i}, \psi_{\rm i})$ plane] of the fields that lead to successful inflation. For simplicity, we have assumed initial velocities to be vanishing $\dot\phi_{\rm i} = \dot\psi_{\rm i} = 0$ as their effect can always be mimicked by starting in a different point with vanishing velocities. Then for each initial conditions, we have integrated the equations of motion and computed the field values and the number of e-folds as a function of time. Choosing to end simulations when inflation is violated would have not allowed us to study trajectories where inflation is transiently interrupted as it may happen (see Sec. II A 1). Therefore, we chose to end the numerical integration when the trajectory is sure to be trapped by one of the two global minima, because at that point, no more e-folds will be produced. This is realized when the sum of the kinetic and potential energy of the fields is equal to the height of the potential barrier between the vacua, i.e. when

$$\lambda M^4 = \frac{1}{2}(\dot\phi^2 + \dot\psi^2) + V(\phi, \psi). \quad (16)$$

We have defined "successful inflation" as a period that lasts at least for 60 e-folds.[4]

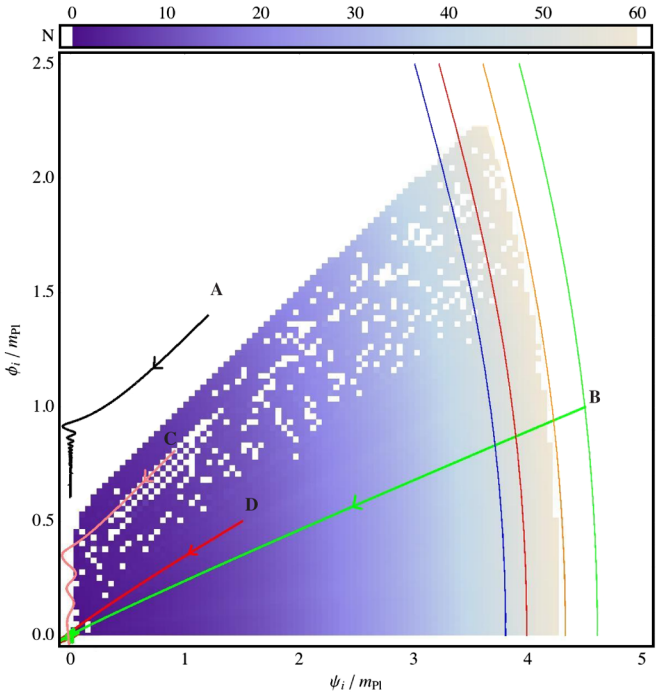

FIG. 4 (color online). Grid of initial conditions leading to successful (white regions) and unsuccessful inflation (colored region), for the original hybrid inflation with $\lambda = \lambda' = 1$, $m = 10^{-6}m_{\rm pl}$ and $M = 0.03m_{\rm pl}$. The color code denotes the number of e-folds realized. Three typical successful trajectories [in the valley (A), radial (B), and from an isolated point (C)] are added as well as an unsuccessful trajectory (point D). Also plotted are the isocurves of ϵ_1, in the slow-roll approximation, for $\epsilon_1 = 0.022$, 0.02, 0.0167 and 0.015 (from left to right).

[3] $a_{\rm i}$ is the scale factor at the beginning of inflation.

[4] Note that the number of e-folds required to solve the horizon problem actually depends on the energy at which inflation is realized or the reheating temperature [9,59,60]

$$N_{\rm horizon} = 62 - \ln(10^{16}\ {\rm GeV}/V_{\rm end}^{1/4}) - \frac{1}{3}\ln(V_{\rm end}^{1/4}/\rho_{\rm reh}^{1/4}).$$

Here we will assume that inflation takes place at high energy, close to the GUT scale.

Let us mention that our aim here is not to provide the best fit to the cosmological data but to explore the space of initial conditions that lead to sufficient inflation within the hybrid class of models. However, notice that the COBE normalization can always be achieved by a rescaling of the potential without affecting the inflaton dynamics.

In Fig. 4 the grid of initial values is presented for the original hybrid inflation model of Eq. (1). For values of parameters comparable to those used in [29,31], we have put in evidence three types of trajectories in the fields space to obtain successful inflation. An example of each has been represented in Fig. 4 and identified by a letter A, B, or C whereas an example of a failed trajectory is identified by a D. The details of these trajectories are represented in Fig. 5 where the values of the fields for three trajectories are plotted as a function of the number of e-folds. A more detailed description of the more interesting type-C trajectory is represented separately in Fig. 6. Each trajectory is described and explained below.

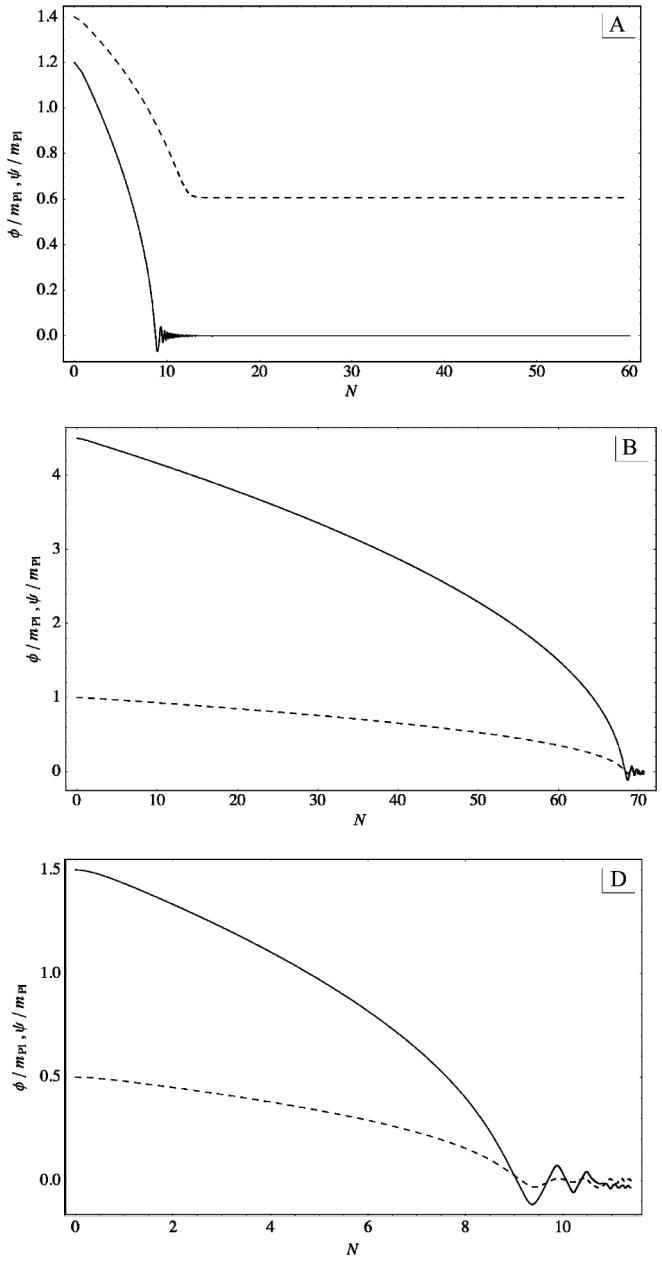

FIG. 5. Evolution of the fields ϕ (dashed lines) and ψ (plain lines) with the number of e-folds realized, for the trajectories A, B, and D (from top to bottom) as represented in Fig. 4. The more interesting type-C trajectory is represented in Fig. 6 below.

Trajectory A: along the valley.—This region of successful inflation corresponds to a narrow band along the $\psi = 0$ line and is the standard evolution. Trajectories are characterized first by damped oscillations around the inflationary valley which does not produce a significant number of e-folds. However once the oscillations are damped, the evolution is identical to the one for the effective one-field potential and inflation becomes extremely efficient in terms of e-folds created. This explains the abrupt transition between the unsuccessful and the successful type-A regions observed in Fig. 4. Indeed, unsuccessful points with around 10 e-folds created can be found right next to the white successful region where $N \gg 60$. The difference between two close points in each region is that for the successful one, the system just has the right amount of time for the oscillations to become damped before entering the global minimum where inflation ends.

For larger initial values of the ϕ field (around and above the Planck mass), the narrow band of successful inflation opens up and inflation is always successful (in agreement with [29,30]. In this region (at the top of Fig. 4), it is always possible for the oscillations to become damped and for the efficient regime of inflation to start before the end of inflation: *the fine-tuning on the initial conditions disappears at large values of ϕ for any values of ψ*. This behavior is similar to the chaotic inflation model, where

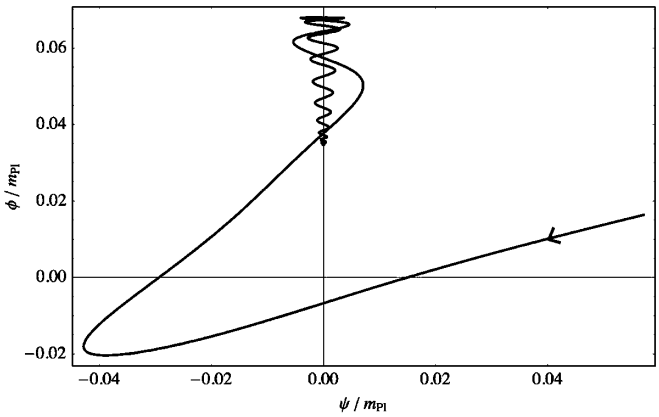

FIG. 6. More detailed description of the field values during a type-C trajectory as defined in Fig. 4. This is a zoom of the trajectory close to the bottom of the potential. One can notice that the system quickly rolls down while few e-folds are produced before ''accidently'' climbing up the valley. Then it starts a second efficient phase of inflation like a type-A trajectory.

[61] super-Planckian values are necessary to have a long enough inflationary phase.

By comparing the time necessary for the expansion to damp the oscillations and the time taken by the inflaton to reach the critical point of instability, an analytical approximation of the width ψ_w of the narrow successful band has been proposed in [29],

$$\psi_w \simeq \sqrt{\frac{3\lambda\pi^3}{4\lambda'}}\frac{M^2}{m_{pl}}. \quad (17)$$

For the parameter values of the Fig. 4, $\psi_w \sim 4\times 10^{-3} m_{pl}$. This provides a good fit of the width of the inflationary valley at small $\phi \ll m_{pl}$. This successful band is so thin that quantum fluctuations would have an amplitude large enough to shift the field ψ outside the successful band [29]. For larger initial values of ϕ, it is also possible to provide an analytical fit of the limit successful/unsuccessful. Figure 4 suggests that the limit $\phi_{lim}(\psi)$ is a linear function. From a given set of initial conditions (ϕ_i, ψ_i), the total number of e-folds generated depends almost only on the value $\phi = \phi_{hit}$ at which the oscillations in ψ become damped and the slow-roll starts in the valley. The reason is that a type-A trajectory rolls faster before ϕ_{hit} and thus does not generate many e-folds before the valley. As a consequence, the limit between successful and unsuccessful regions necessarily follows the unique trajectory for which ϕ_{hit} becomes large enough to generate exactly 60 e-folds by slow-roll in the valley. As a result, using the slow-roll approximation, the slope of the limit is simply given by the gradient of the potential

$$\alpha = \frac{\partial V(\phi,\psi)/\partial\phi}{\partial V(\phi,\psi)/\partial\psi} \simeq \frac{\lambda'\phi\psi}{\lambda\psi^2+\lambda'\phi^2}, \quad (18)$$

where the approximated expression is valid when mass parameters are small $\psi \gg \max(m, m/\lambda')$. Given one point of the transition line, for example, (1, 1), we can check that the slope of the limit is $\alpha \simeq 0.5$ for the parameters of Fig. 4.

Trajectory B: radial.—Enlarging the space of initial conditions to super-Planckian values shows another region where successful inflation is automatic. It is observed for super-Planckian initial values of the auxiliary field ψ beyond a few Planck mass, in a way reminiscent to the chaotic scenario. In this case, the trajectory is called radial and the 60 e-folds are realized mostly before reaching the valley or the global minima.

From the ϕ-axis to larger values of ψ_i, the number of e-folds realized increases slowly (see Fig. 4). Therefore, this limit between the two regions is smooth unlike the limit with A-type trajectories described at the previous paragraph. Increasing ϕ_i, the critical value of ψ_i leading to enough inflation decreases slowly, because inflation is radial and the trajectory longer. To describe this limit more precisely, we have plotted the isocurves of ϵ_1 in Fig. 4) in the two-fields slow-roll approximation. We can see that this limit follows one of these isocurves, namely $\epsilon_1 \simeq 0.0167$. This observation can be understood using a kinematic analogy [60] as long as ϵ_2 is negligible. This critical value of ϵ_1 can be computed analytically, by studying the easiest trajectory of this kind at $\phi_i = 0$. In this case, the effective potential is dominated by $\lambda\psi^4$, and the critical ψ_i is obtained by requiring a phase of inflation of exactly $N_{suc} = 60$ e-folds. We find

$$\psi_{ic} = \sqrt{\frac{m_{pl}^2}{\pi}N_{suc}} \approx 4.37 m_{pl}. \quad (19)$$

At this value, the corresponding first Hubble-flow parameter ϵ_{1c} reads

$$\epsilon_{1c} \simeq \frac{1}{N_{suc}} \approx 0.0167. \quad (20)$$

Trajectory C and D: isolated successful points and unsuccessful points.—Previous works [29,31] pointed out the presence of unexplained successful isolated points in the central unsuccessful region. In this paragraph, we justify their existence, study their properties and quantify the area they occupy.

Let us first describe the D-type trajectories that are unsuccessful. As shown in Fig. 5, in these cases, the system quickly rolls down the potential to one of the global minima of the potential during which only a few e-folds are created. What is then the difference between the D-type and the C-type trajectories plotted in Fig. 6 ? The fields roll towards the bottom of the potential with sufficient kinetic energy and, after some oscillations close to the bottom of the potential, the momentum is ''by chance'' oriented toward the inflationary valley. Thus the system goes up the valley until it looses its kinetic energy and then starts slow-rolling back down the same valley producing inflation with a large number of e-folds. Note that there are more of these points in a band under the limit of type-A trajectories. This is because, at higher ϕ_i, there are more chances to find a trajectory where the momentum at the bottom of the potential is oriented toward the inflationary valley.

High resolution grids and zooms on peculiar regions of Fig. 4 show that these apparently random isolated points form actually a complex structure. Some of it, for small initial conditions, is visible in Fig. 7. The points are organized in long thin lines, or croissants. The points that seem isolated actually belong to structures that a better resolution would show continuous. Some of our biggest structures can be identified also in [29] but are not recovered in [31] where only isolated points were found. This may be explained by the need of a higher resolution to resolve the structures. A detailed analysis of trajectories shows that for each continuous successful region corresponds a unique number of crossings the $\phi = 0$ axis by the trajectory before climbing up and going back down the inflationary valley along the $\psi = 0$ direction.

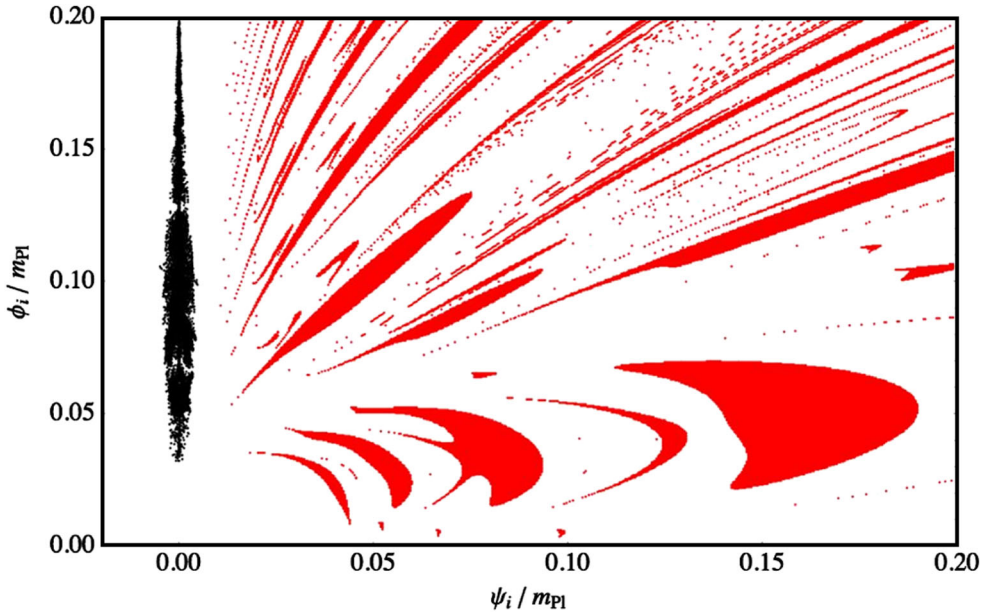

FIG. 7 (color online). Structure of the successful "anamorphosis points" (in red/grey) together with their images (in black) defined by the point of the trajectory at which the velocities of the fields vanish. The structure in grey can be seen as the anamorphosis of the patterns of successful inflation in black. In this analogy the trajectories of the light on the optic device in order to create a meaningful image are replaced by the trajectories of the system in field space to create a meaningful image (in the valley) from the apparently senseless grey patterns. This is obtained for $M = 0.03 m_{\rm pl}$, $m = 10^{-6} m_{\rm pl}$, $\lambda = \lambda' = 1$.

For each of these type-C trajectories, we can identify the point (that we will call the "image") on the inflationary valley at which the velocities of the fields become (quasi) null. We show the robustness of the previous description of the type-C trajectories, by observing that all these images are in the successful narrow band responsible for the type-A trajectories. More precisely, the images obtained populate *exactly* the narrow band of width ψ_w as described in Eq. (17). As a conclusion each successful point in the unsuccessful region corresponds to a point in the narrow successful band. The identification between the isolated points and their images in the inflationary valley is represented in Fig. 7, when restricting ourselves positive initial field values. Using the analogy with optical *anamorphosis*, we can say that the observed structures of type-C initial conditions generates by anamorphosis the successful narrow band around the inflationary valley. In this analogy, the potential plays the role of the optical instrument used to create the meaningful image. The trajectories of the light rays on the optic device are then replaced by the field trajectories to create a meaningful image (in the valley) from the apparently senseless patterns of successful initial conditions.

Let us elaborate a little more on the properties of the images in Fig. 7. Since the potential is invariant under $\phi \rightarrow -\phi$, there exist two different inflationary valleys, one going toward $\phi > 0$ and one going $\phi < 0$. Some of these type-C initial conditions give rise to inflation thanks to the first valley when the others will realize inflation in the second. Obviously the two situations are equivalent and symmetric, just like the value of the initial conditions that could be taken in the negative planes (with $\phi_i < 0$ or $\psi_i < 0$ or both). It is clear that these additional planes contain identical patterns and some of these initial conditions would populate as well the inflationary valley represented above. Moreover, the set of images in the valley represented in Fig. 7 is not of constant width as it should be for another reason. The initial conditions represented are restrained below $M_{\rm pl}$ but the structures observed continue at larger values. The trajectories starting with these larger values of ϕ_i would have the momentum to climb up the valley more and populate the higher part of the set of images.

4. Dependencies on the parameters

The grid of initial conditions, and therefore the proportion of successful points in a given range of initial values naturally depend on the values of the parameters of the potential. Three physical quantities are of interest to study these evolutions: the width of the inflationary valley, proportional to $M\sqrt{\lambda/\lambda'}$, its length controlled by the critical value $\phi_c = M\sqrt{\lambda/\lambda'}$, the depth of the global minima of the potential given by $V_0 \propto \lambda M^4$, and the gradient of the potential $\alpha \simeq \lambda'/(\lambda + \lambda')$.

Evolution of the limit of A-type trajectories.—At small ϕ, a smaller λ induces a narrower inflationary valley, and therefore fewer successful initial conditions. At large ϕ, the slope α in Eq. (18), is mostly a function of the coupling constants. For a smaller value of λ, the slope of the limit

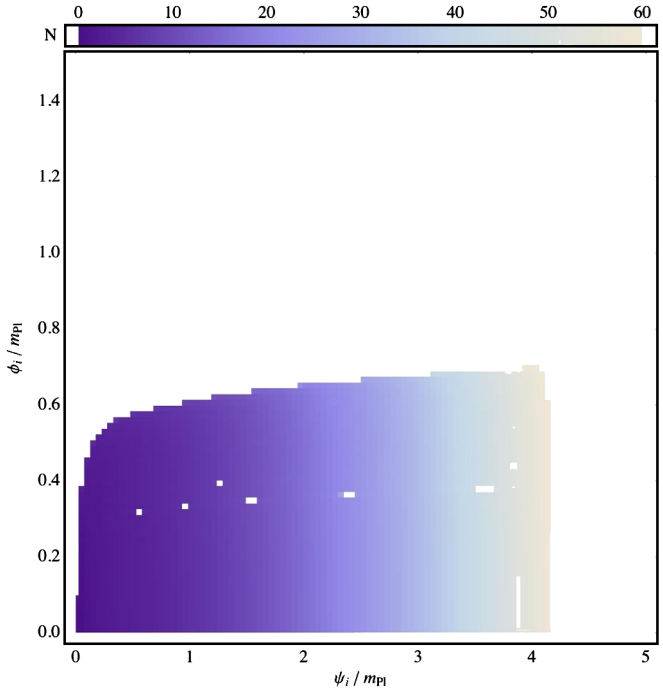

FIG. 8 (color online). Grid of initial conditions, for hybrid potential with $M = 0.03 m_{\rm pl}$, $m = 10^{-6} m_{\rm pl}$, $\lambda = 1$, $\lambda' = 0.1$.

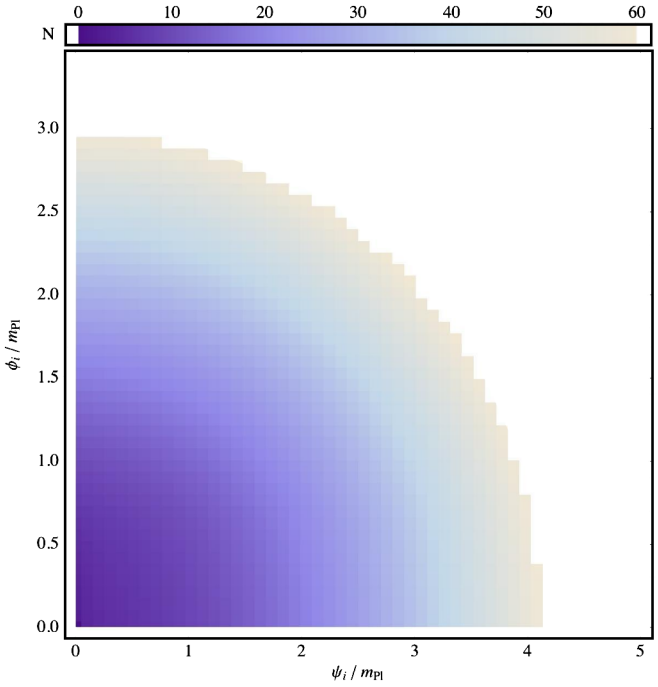

FIG. 9 (color online). Grid of initial conditions and example trajectories for the hybrid model, with $m = M = 10^{-3} m_{\rm pl}$, $\lambda = 1$, $\lambda' = 10^{-2}$.

increases. For smaller value of λ', the slope of the limit is reduced as represented on Fig. 8. This effect is due to the potential now dominated by the $\lambda\psi^4$ term, depending less on ϕ. Thus the velocity in the ψ direction is enhanced compared to the ϕ one.

As long as the mass squared m^2 is subdominant compared to $\lambda'\psi^2$, its variation do not affect the properties of the initial condition plane. Increasing the mass m above this limit increases the velocity in the ϕ direction and tends to spoil the slow-roll evolution in the inflationary valley. As already described in Sec. II A 1, this violation of the slow-roll conditions in the valley imposes for inflation to occur in the large field phase. In the space of initial conditions, the narrow successful band then disappear together with the type-C trajectories. Finally the unsuccessful region takes an elliptic form as represented in Fig. 9, with a smooth transition between successful and unsuccessful regions. The model becomes comparable to the sum of two chaotic inflation models and we recover the feature of these models: it is almost unavoidable to have super-Planckian initial values of the fields to realize a sufficiently long inflation.

Evolution of the amount of C-type trajectories.—A similar explanation can be given to justify the absence of isolated points for small values of λ' (see Fig. 8). Even though the width of the valley is larger, the potential is then dominated by the $\lambda\psi^4$ term and the ϕ-component of the velocity becomes small. Thus the chances for the system to climb up the valley are suppressed. For larger values of the parameters M and λ, these isolated points also disappear, because the two minima of the potential are deeper, and

TABLE I. Percentage of successful points in grids of initial conditions, for different values of parameters, when restricting to $\phi_{\rm i}$, $\psi_{\rm i} \leq M_{\rm pl}$. The third column represents the area of the whole successful initial condition parameter space over the total surface. The fourth column represents the surface of the successful space only located in isolated points, over the total surface. This allows to visualize the importance of these isolated points. For several of these sets of values for the potential parameters, the grid of initial conditions is represented in the body of the paper. When it is the case, the number of the figure is given in column 5.

Model	Values of parameters	Successful points (%)	Anamorphosis points (%)	Figure
Hybrid	$M = 0.03 m_{\rm pl}$, $m = 10^{-6} m_{\rm pl}$, $\lambda = \lambda' = 1$	17.4	14.8	4
Hybrid	$M = 0.06 m_{\rm pl}$, $m = 10^{-6}$, $\lambda = 1$, $\lambda' = 1$	11.3	5.5	
Hybrid	$M = 0.03 m_{\rm pl}$, $m = 10^{-5} m_{\rm pl}$, $\lambda = \lambda' = 1$	17.4	14.8	
Hybrid	$M = 0.03 m_{\rm pl}$, $m = 10^{-6} m_{\rm pl}$, $\lambda = 0.1$, $\lambda' = 1$	15.5	14.1	
Hybrid	$M = 0.03 m_{\rm pl}$, $m = 10^{-6} m_{\rm pl}$, $\lambda = 1$, $\lambda' = 0.1$	2.8	<0.1	8
Hybrid	$M = m = 10^{-3} m_{\rm pl}$, $\lambda = 1$, $\lambda' = 10^{-2}$	0	0	9

there is a larger chance for the system to get trapped in them without climbing up the inflationary valley. These results are summarized in Table I below.

Quantification of successful initial conditions.—We end this section by quantifying what proportion of the initial condition space give rise to inflation for hybrid inflation, for various values of the parameters, including the proportion of points in the anamorphosis. Our results are represented in Table I, where the quantification is first made restricting the amplitude of the fields below the reduced Planck mass. From this table, we can see that unless λ' is very small, or M is close to Planckian values, the hybrid model possesses about 15% of initial conditions that leads to successful inflation. For this percentage to be translated into a probability of realizing inflation, one would need a measure in the probability space. If this measure was to be flat, *the successful initial conditions should not be considered as fine-tuned but simply subdominant when fields are restricted to sub-Planckian values*.

From Fig. 4, it is obvious that if we do not require that the fields are smaller than the reduced Planck mass, the proportion of successful initial conditions will tend toward 100%. Therefore, we have also realized the same quantification with the requirement $\phi_i, \psi_i \leq 5m_{\rm pl}$ and found that the percentage of successful initial conditions raise to 72% for the parameter values of Fig. 4.

III. INITIAL CONDITIONS FOR EXTENDED MODELS OF HYBRID INFLATION

In this section, we will study the properties of initial conditions leading to successful inflation for three hybrid-type models of inflation and study how generic the properties observed for the original model are. The models are the smooth, and shifted hybrid inflation both in global SUSY and SUGRA, and radion inflation.

A. Motivations for smooth and shifted hybrid inflation

Following the original inflation model, a supersymmetric formulation, the F-term hybrid inflation, has been proposed by [17]. In this case, the inflaton field ϕ is replaced by a superfield S, and the Higgs field ψ is replaced by a pair of Higgs superfields $\bar{\Phi}$, Φ nontrivially charged under a symmetry group[5] G whereas S is assumed to be a gauge singlet of G. The only superpotential, invariant under G and under an R-symmetry[6] and containing only renormalizable terms reads [17]

$$W^F = \kappa S(\Phi_+\Phi_- - M^2). \tag{21}$$

It gives rise to a scalar potential similar to Eq. (1), the coupling constants λ and λ' being replaced by κ. This potential possesses the same features with the inflationary valley along $\bar{\Phi}$, $\Phi = 0$, this valley being destabilized when one of the superfields $\bar{\Phi}$, Φ becomes tachyonic. The field develops a nonvanishing vev which leads to the breaking of G. Topological defects can be produced during this breaking, depending on G. They can be cosmic strings [20] which would be in agreement with the most recent CMB data [62–64], provided that their effect on the CMB is subdominant [65]. But they could also be monopoles or domain walls and then be in contradiction with observations [66].

To be able to implement hybrid inflation at any symmetry breaking, it has been proposed two extensions of the F-term model: the smooth [39] and the shifted [42] hybrid inflation. They are both based on the idea of shifting the inflationary valley away from $\psi = 0$. As a consequence the symmetry G is broken *during or before* inflation, and thus any topological defect formed during this breaking are diluted away by inflation. This is achieved by introducing nonrenormalizable terms in the potential [39,42] and imposing an additional discrete symmetry for the superpotential [39].

As detailed in the introduction, if these models are considered realistic, that is if the scalar potential is assumed to be originated from SUSY or SUGRA, it is not safe to consider super-Planckian fields. It can also be safe to study these models beyond super-Planckian fields if they originate from other frameworks where nonrenormalizable corrections are controlled or prevented.

B. Smooth inflation

1. The potential in SUSY

Smooth inflation has been introduced by Lazarides and Panagiotakopoulos [39]. It assumes that the superpotential is invariant under a Z_2 symmetry under which $\Phi\bar{\Phi} \rightarrow -\Phi\bar{\Phi}$. This forbids the first term in the F-term superpotential of Eq. (21) but allows for one nonrenormalizable term[7] [39]

$$W^{\rm sm} = \kappa S\left[-M^2 + \frac{(\bar{\Phi}\Phi)^2}{M_{\rm pl}^2}\right]. \tag{22}$$

In the context of global supersymmetry, the scalar potential reads [39]

$$V^{\rm sm}(S,\Phi,\bar{\Phi}) = \kappa^2\left|-M^2 + \frac{(\bar{\Phi}\Phi)^2}{M_{\rm pl}^2}\right|^2 + 4\kappa^2|S|^2\frac{|\Phi|^2|\bar{\Phi}|^2}{M_{\rm pl}^4}(|\Phi|^2 + |\bar{\Phi}|^2), \tag{23}$$

[5]They are assumed to belong to two complex conjugate representations.

[6]This R-symmetry is a $U(1)$ symmetry under which Φ and $\bar{\Phi}$ have opposite charges and S and W have identical charges.

[7]Note that our choice of setting the renormalization scale to the reduced Planck mass is arbitrary. In general, we can write $W^{\rm sm} = \kappa S[-M^2 + (\bar{\Phi}\Phi)^2/\Lambda^2]$, Λ corresponding to the scale of new physics.

where we denote by the same letter the superfields and their scalar components. Two real scalar fields ϕ and ψ can be defined as the relevant components of the S, Φ, $\bar{\Phi}$ fields such that the fields are canonically normalized

$$\phi \equiv \sqrt{2}\,\mathrm{Re}(S), \qquad \psi \equiv 2\,\mathrm{Re}(\Phi) = 2\,\mathrm{Re}(\bar{\Phi}), \tag{24}$$

and the potential becomes [39]

$$V^{\mathrm{sm}}(\phi, \psi) = \kappa^2\left(M^2 - \frac{\psi^4}{16M_{\mathrm{pl}}^2}\right)^2 + \kappa^2\phi^2\frac{\psi^6}{16M_{\mathrm{pl}}^4}. \tag{25}$$

This potential contains a flat direction $\psi = 0$, but it is a local maximum. The global minima are obtained for non-vanishing values of ψ: they define two distinct inflationary valleys, along

$$\psi = \pm\sqrt{-6\phi^2 + 6\sqrt{\phi^4 + \frac{4}{9}M^2M_{\mathrm{pl}}^2}}. \tag{26}$$

Note that these inflationary valleys progressively shift away from $\psi = 0$ as ϕ evolves towards 0.

2. Space of initial conditions

In a previous study by Lazarides *et al.* [32], an exploration of the space of initial conditions leading to sufficient inflation was performed, with a low resolution. This exploration led to a conclusion opposite to the one found for the nonsupersymmetric hybrid inflation model: most of the space was found to be successful. Therefore, smooth hybrid inflation seems a good laboratory to test the validity of the results we found at the previous section. We performed the exploration of the space of initial conditions, for a higher resolution, and for a larger range of initial field values and parameter values. Imposing ϕ_i, $\psi_i \leq M_{\mathrm{pl}}$, we computed the proportion of successful initial conditions and the proportion of isolated successful points away from the inflationary valleys.

Our study, also extended to super-Planckian values of the fields, always reveals a structure similar to that of the original model. We observe (see for e.g. Fig. 10) a narrow band of fine-tuned successful initial conditions along $\psi = 0$, a triangular unsuccessful region, and successful areas for large initial values of one or both of the fields. Anamorphosis is also present, leading to isolated successful patterns in the unsuccessful region. For the values of the parameters quoted in Ref. [32], that is with a mass scale of order $10^{-5}m_{\mathrm{pl}}$, they occupy most of the space of initial condition as shown on Fig. 10. We find almost 80% of initial conditions below the reduced Planck mass to be successful.

We have also studied how this grid evolves with the parameters of the potential. We first observe that the amount of successful initial conditions is independent of the coupling constant κ (it only scales the potential or the CMB spectrum), but only depends on the mass scale M.

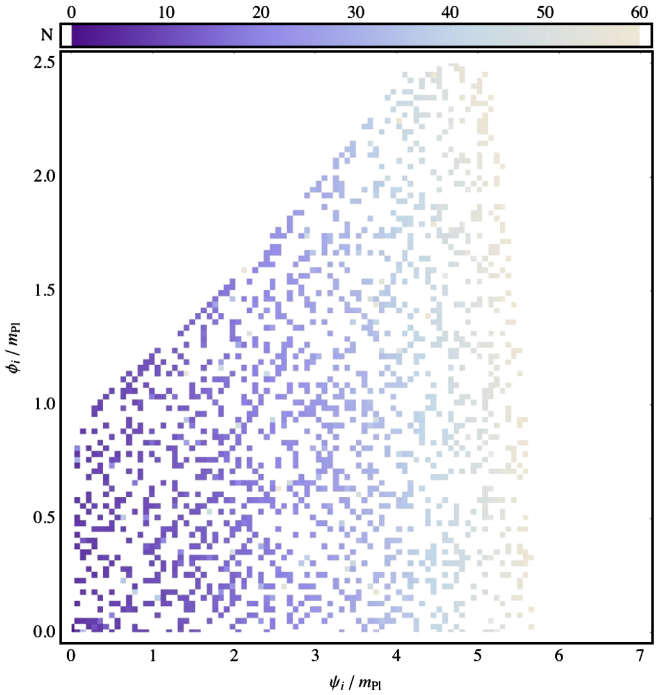

FIG. 10 (color online). Grid of initial conditions for smooth inflation, using the values of the parameters of [32]: $\kappa \simeq 10$, $M \simeq 2.3 \times 10^{-5}m_{\mathrm{pl}}$.

This analysis shows a strong dependency with the value of M, the amount of successful initial conditions ranging from 15% to almost 80% when M ranges from 10^{-2} and 10^{-5}. For M below the GUT scale, 10^{16} GeV, the quantification of successful initial conditions is larger than 50%, providing a good mechanism to produce inflation without fine-tuning of initial conditions. As a conclusion, we confirm the qualitative results of [32], and we note that they depend on the values of potential parameters. We note also that most of the successful initial conditions are isolated, that is located outside of the inflationary valleys: they form an anamorphosis like in the hybrid inflation model. These results are summarized in the Table II at the end of this section.

3. Supergravity corrections

The smooth hybrid inflation is based on a superpotential that contains a nonrenormalizable term, with a cutoff scale chosen at the reduced Planck mass. In addition, in our study we consider field values that are non-negligible compared to M_{pl}, sometimes above. Therefore, to extend the domain of validity of the model, supergravity corrections (introducing corrections proportional to negative powers of M_{pl}) should be taken into account. We remind the reader that outside of the domain of validity of the model (whether in SUSY or in SUGRA), the model is still studied but considered as an effective model derived from some frameworks in which super-Planckian field values can safely be considered (see introduction).

TABLE II. Percentage of successful points in grids of initial conditions, for different models and values of parameters, when restricting to ϕ_i, $\psi_i \leq M_{pl}$. The third column represents the area of the whole successful initial condition parameter space over the total surface. The fourth column represents the surface of the successful space only located in isolated points, over the total surface. Some of these sets are represented in the body of the paper, the relevant figure being reported in last column.

Model	Values of parameters	Successful points (%)	Isolated points (%)	Figure
Hybrid	$M = 0.03m_{pl}$, $m = 10^{-6}m_{pl}$, $\lambda = \lambda' = 1$	17	15	4
Hybrid	$M = 0.06m_{pl}$, $m = 10^{-6}$, $\lambda = 1$, $\lambda' = 1$	11	6	
Hybrid	$M = 0.03m_{pl}$, $m = 10^{-5}m_{pl}$, $\lambda = \lambda' = 1$	17	15	
Hybrid	$M = 0.03m_{pl}$, $m = 10^{-6}m_{pl}$, $\lambda = 0.1$, $\lambda' = 1$	16	14	
Hybrid	$M = 0.03m_{pl}$, $m = 10^{-6}m_{pl}$, $\lambda = 1$, $\lambda' = 0.1$	3	<1	8
Hybrid	$M = m = 10^{-3}m_{pl}$, $\lambda = 1$, $\lambda' = 10^{-2}$	0	0	9
Smooth	$M = 10^{-2}m_{pl}$, $\kappa = 1$	16	9	
Smooth	$M = 10^{-3}m_{pl}$, $\kappa = 1$	53	49	
Smooth	$M \approx 2.37 \times 10^{-5}m_{pl}$, $\kappa \approx 10.3$	78	60	10
Smooth SUGRA	$M = 10^{-2}m_{pl}$, $\kappa = 1$	29	17	
Smooth SUGRA	$M = 10^{-5}m_{pl}$, $\kappa = 1$	70	70	
Shifted	$M = 0.1m_{pl}$, $\kappa^2 = 1$, $\beta = 0.1m_{pl}^{-2}$	6	<1	12
Shifted	$M = 10^{-2}m_{pl}$, $\kappa^2 = 1$, $\beta = 0.1m_{pl}^{-2}$	15	14	
Shifted	$M = 10^{-2}m_{pl}$, $\kappa^2 = 1$, $\beta = 1m_{pl}^{-2}$	14	13	
Shifted SUGRA	$M = 0.1m_{pl}$, $\kappa^2 = 1$, $\beta = 0.1m_{pl}^{-2}$	<1	<1	
Shifted SUGRA	$M = 10^{-2}m_{pl}$, $\kappa^2 = 1$, $\beta = 0.1m_{pl}^{-2}$	13	12	
Shifted SUGRA	$M = 10^{-2}m_{pl}$, $\kappa^2 = 1$, $\beta = 1m_{pl}^{-2}$	13	12	
Radion	$\psi_0 = 10^{-2}m_{pl}$, $\lambda = 10^{-3}$, $f = 1m_{pl}$	<0.1	<0.1	
Radion	$\psi_0 = 10^{-2}m_{pl}$, $\lambda = 10^{-4}$, $f = 1m_{pl}$	9.4	9.4	
Radion	$\psi_0 = 10^{-2}m_{pl}$, $\lambda = 10^{-5}$, $f = 1m_{pl}$	25.6	24.8	13

Assuming supergravity with a minimal Kähler potential,

$$K = K_{\min} = |\Phi|^2 + |\bar{\Phi}|^2 + |S|^2, \tag{27}$$

the scalar potential reads,

$$V^{sm}_{SUGRA}(S, \Phi, \bar{\Phi}) = \kappa^2 \mathrm{Exp}\left[\frac{K_{\min}}{M_{pl}^2}\right]\left\{\left|\frac{(\bar{\Phi}\Phi)^2}{M_{pl}^2} - M^2\right|^2\left(1 - \frac{|S|^2}{M_{pl}^2} + \frac{|S|^4}{M_{pl}^4}\right) + \frac{|S|^2}{M_{pl}^4}\left[\left(\left|\frac{(\bar{\Phi}\Phi)^2}{M_{pl}^2} - M^2\right|^2 + 4|\Phi|^2|\bar{\Phi}|^2\right)(|\Phi|^2 + |\bar{\Phi}|^2) + 4\Phi^2\bar{\Phi}^2\left(\frac{(\bar{\Phi}^*\Phi^*)^2}{M_{pl}^2} - M^2\right) + \text{c.c.}\right]\right\}. \tag{28}$$

This potential is in agreement with [41], though all terms have here been kept since in our study, fields are not necessarily small compared to the Planck mass. We define again the inflaton and waterfall fields like in Eq. (24), and we obtain the full potential in SUGRA,

$$V^{sm}_{SUGRA}(\phi, \psi) = \kappa^2 \mathrm{Exp}\left[\frac{\phi^2 + \psi^2}{2M_{pl}^2}\right]\left\{\left(M^2 - \frac{\psi^4}{16M_{pl}^2}\right)^2\left(1 - \frac{\phi^2}{2M_{pl}^2} + \frac{\phi^4}{4M_{pl}^4} + \frac{\phi^2\psi^2}{4M_{pl}^4}\right) + \frac{\phi^2\psi^6}{16M_{pl}^4} - \frac{M^2\phi^2\psi^4}{4M_{pl}^4} + \frac{\phi^2\psi^8}{64M_{pl}^6}\right\}. \tag{29}$$

SUGRA corrections induce a steeper potential in the large field regime. We have studied for this last potential the space of initial condition leading to enough inflation and compared the results to the SUSY case. We observe two properties of the space of initial conditions. First, at low initial field values, the initial condition space is mostly unchanged because the correction are small. In particular, the patterns of isolated successful initial conditions still exist and are as numerous. This can be understood because even if SUGRA corrections induce higher velocities for the fields, the anamorphosis mechanism can take place just as easily: the fields fast-roll down the potential, oscillate more around the bottom and sometimes climb up one of the inflationary

valleys. When the fields slow-roll back down the valleys, enough inflation is generated. We note that the probabilities to realize inflation this way are higher in SUGRA than in SUSY and the total and can be as high as 70% for small values of M. Second, the steepness of the potential induces a violation of slow-roll for radial trajectories leading first to a smaller probability to realize inflation directly starting in the inflationary valleys because they become more narrow. Second we do not observe automatic successful inflation at large super-Planckian initial field values and similar patterns of isolated points are observed instead.

C. Shifted inflation

1. The potential

The shifted inflation model, proposed by Jeannerot *et al.* [42], is similar to the smooth inflation model, but the additional Z_2 symmetry of smooth inflation is not imposed anymore. Thus the superpotential reads

$$W^{\mathrm{sh}} = \kappa S\left(-M^2 + \bar{\Phi}\Phi - \beta\frac{(\bar{\Phi}\Phi)^2}{M_{\mathrm{pl}}^2}\right). \tag{30}$$

This gives rise to the following F-terms contributions to the scalar potential, in the context of global supersymmetry

$$V^{\mathrm{sh}}(S,\Phi,\bar{\Phi}) = \kappa^2\left\{\left|-M^2 + \bar{\Phi}\Phi - \beta\frac{(\bar{\Phi}\Phi)^2}{M_{\mathrm{pl}}^2}\right|^2 + |S|^2(|\bar{\Phi}|^2 + |\Phi|^2)\left|1 - 2\beta\frac{\bar{\Phi}\Phi}{M_{\mathrm{pl}}^2}\right|^2\right\}, \tag{31}$$

where we have used the same letter to denote the superfields and their scalar component. We can define the relevant fields $\bar{\psi}$ and ψ as the components of $\bar{\Phi}$ and Φ that

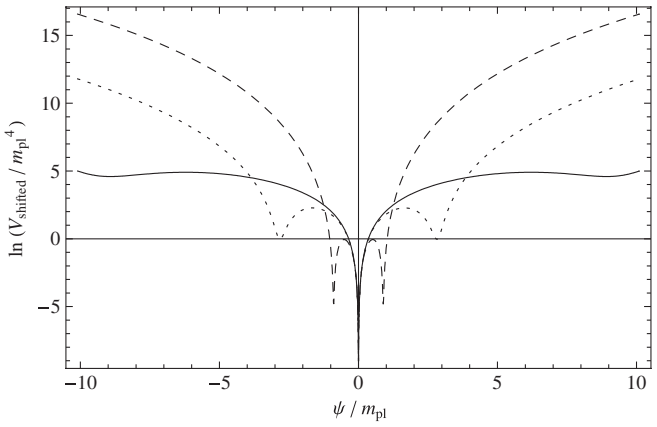

FIG. 11. Cut of the logarithm of the shifted potential $V^{\mathrm{sh}}(\phi,\psi)$, at $\phi = 2m_{\mathrm{pl}}$, for $M = 0.1m_{\mathrm{pl}}$, $\kappa = 1$, and $\beta = 10^{-3}m_{\mathrm{pl}}^{-2}$ (plain line), $\beta = 10^{-2}m_{\mathrm{pl}}^{-2}$ (dotted line), $\beta = 10^{-1}m_{\mathrm{pl}}^{-2}$ (dashed line). Notice the appearance of multiple inflationary valleys, whose number and positions depend on the parameter β. They also depend on the value of ϕ.

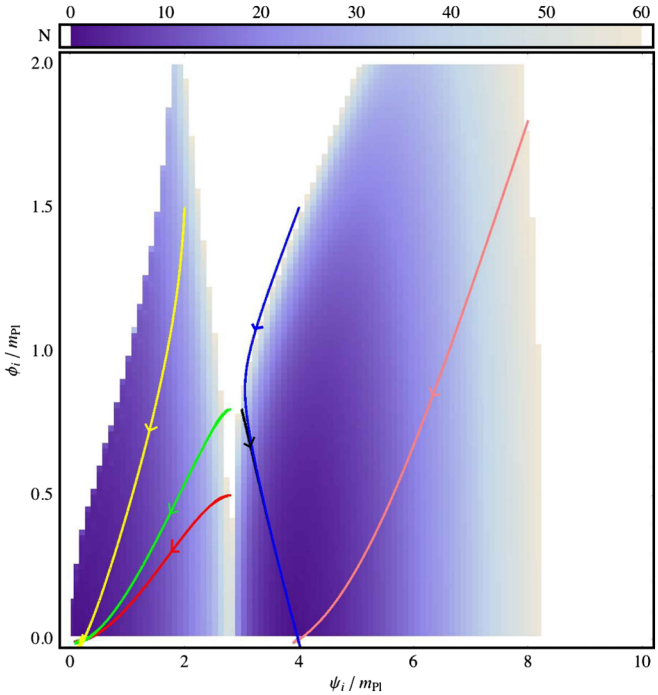

FIG. 12 (color online). Grid of initial conditions leading or not to inflation, for the shifted potential with $M = 0.1m_{\mathrm{pl}}$, $\kappa = 1$, and $\beta = 10^{-2}m_{\mathrm{pl}}^{-2}$. Some trajectories in field space have been represented to identify where local maxima and minima are.

generate the breaking of the group G. We can define the inflaton and waterfall fields like in Eq. (24) so as to vanish the D-term contributions to the potential and to have canonical kinetic terms. The effective scalar potential then becomes [42],

$$V^{\mathrm{sh}}(\phi,\psi) = \kappa^2\left(\frac{\psi^2}{4} - M^2 - \beta\frac{\psi^4}{16M_{\mathrm{pl}}^2}\right)^2 + \frac{\kappa^2}{4}\phi^2\psi^2\left(1 - \beta\frac{\psi^2}{2M_{\mathrm{pl}}^2}\right)^2. \tag{32}$$

In the limit of negligible β, one recovers the same potential as for the original hybrid model with $\lambda = \lambda' = \kappa$, that is with a valley of local minima at $\psi = 0$. As β increases, two symmetric valleys appear, parallel to the central one as represented in Fig. 11.

These new inflationary valleys get closer to the central one as β gets larger. The central valley corresponds to a local minima at large ϕ. It becomes, as ϕ rolls toward 0, a local maxima at which point, two additional valleys appear. Assuming a large ϕ field initially, inflation can be realized along one of the three valleys. Several trajectories for various initial conditions are represented on Fig. 12 to illustrate this. Inflation stops when the fields oscillate and settle in one of the global minima of the potential.

2. Space of initial conditions

Grids of initial conditions leading or not to inflation have been computed; one of them is represented in Fig. 12 for

one set of parameters. It corresponds to one cut of the potential in Fig. 11 (dotted line).

For a small coupling β (say of order 10^{-3}), if we restrict ourselves to values of the waterfall field smaller than $5m_{\rm pl}$, we obtain a space of initial conditions similar to the original hybrid case (see Fig. 4), with a triangular shaped region of unsuccessful inflation surrounded by successful regions at higher values of the fields.

At larger values of ψ, around the new inflationary valley (the shifted one) at a positive ψ, a second triangular shaped unsuccessful region is observed in addition. For example, for $\beta = 10^{-3}m_{\rm pl}^2$, this shifted valley is located at $\psi = 9m_{\rm pl}$ (at $\phi = 2m_{\rm pl}$). Unlike the central one, the shifted valley is too steep to generate inflation when the fields start inside it. Thus no line of successful initial conditions along the valley is observed. Successful inflation is only realized when starting sufficiently far from the valley, when the potential becomes flatter around $\psi \in [3, 8]m_{\rm pl}$ (see Fig. 11).

If we increase β, the shifted valley gets closer to the $\psi = 0$ one. As a consequence, the two unsuccessful regions become closer as well, with interferences between them, as shown in Fig. 12.

The shape of the first unsuccessful region is modified because the presence of the second valley renders some unsuccessful trajectories successful. We have represented some examples of such trajectories in Fig. 12. Finally, note that if this model is not considered as an effective model for which fields can be super-Planckian, in the limit of small β this model reduces to the original hybrid one. Conclusions concerning the relative area of successful points are then the same. For larger values of β though, the new band of successful inflation can appear even below the reduced Planck mass and increase the probability of successful inflation. These results are summarized in Table II.

3. Supergravity corrections

Let us discuss, as for the smooth hybrid model, the effects of embedding the model in supergravity to study the robustness of our conclusions under nonrenormalizable corrections. As discussed in the introduction, we remind the reader that neither supersymmetry nor supergravity is a valid framework for describing super-Planckian fields and in this regime, the models studied are considered as effective models. However supergravity corrections allow to extend the domain of validity up to Planckian-like field values.

The supergravity corrections to the shifted potential are computed assuming again a minimal Kähler potential and we obtain,

$$V_{\rm SUGRA}^{\rm sh}(S,\Phi,\bar{\Phi}) = \kappa^2 {\rm Exp}\left[\frac{K_{\rm min}}{M_{\rm pl}^2}\right]\left\{\left|\bar{\Phi}\Phi - M^2 - \beta\frac{(\bar{\Phi}\Phi)^2}{M_{\rm pl}^2}\right|^2\left(1 - \frac{|S|^2}{M_{\rm pl}^2} + \frac{|S|^4}{M_{\rm pl}^4}\right)\right.$$
$$+ |S|^2(|\Phi|^2 + |\bar{\Phi}|^2)\left[\left|1 - 2\beta\frac{\bar{\Phi}\Phi}{M_{\rm pl}^2}\right|^2 + \frac{1}{M_{\rm pl}^4}\left|\bar{\Phi}\Phi - M^2 - \beta\frac{(\bar{\Phi}\Phi)^2}{M_{\rm pl}^2}\right|^2\right]$$
$$\left. + 2\frac{|S|^2}{M_{\rm pl}^2}\left[\Phi\bar{\Phi}\left(1 - 2\beta\frac{\Phi\bar{\Phi}}{M_{\rm pl}^2}\right)\left(\bar{\Phi}^*\Phi^* - M^2 - \beta\frac{(\bar{\Phi}^*\Phi^*)^2}{M_{\rm pl}^2}\right) + {\rm c.c.}\right]\right\}. \quad (43)$$

By defining the inflaton and the waterfall field to be the canonically normalized real part of the fields S, Φ, and $\bar{\Phi}$ like in the SUSY case, we obtain the effective 2-field potential,

$$V_{\rm SUGRA}^{\rm sh} = \kappa^2 {\rm Exp}\left(\frac{\phi^2 + \psi^2}{2M_{\rm pl}^2}\right)\left\{\left(\frac{\psi^2}{4} - M^2 - \beta\frac{\psi^4}{16M_{\rm pl}^2}\right)^2\left(1 - \frac{\phi^2}{2M_{\rm pl}^2} + \frac{\phi^4}{4M_{\rm pl}^4}\right)\right.$$
$$\left. + \frac{\phi^2\psi^2}{4}\left[1 - \beta\frac{\psi^2}{2M_{\rm pl}^2} + \frac{1}{M_{\rm pl}^2}\left(\frac{\psi^2}{4} - M^2 - \beta\frac{\psi^4}{16M_{\rm pl}^2}\right)\right]^2\right\}. \quad (34)$$

These corrections affect at large initial values of the fields the dynamic of inflation. At super-Planckian initial values, the exponential term dominates and the potential become too steep for inflation to be automatically realized like in the SUSY case. However, the anamorphosis (or type-C) trajectories still exist and are still the main origin of successful inflation. We have computed for several sets of the parameters the percentage of successful initial conditions taking into account these corrections. We do not find significant modifications compared to the SUSY case except at large mass scale, where the steepness of the potential prevents from inflation to be successful in the valleys. These results are summarized in Table II.

D. Radion assisted gauge inflation

1. Motivations

As mentioned in the introduction, the ''radion inflation'' model [24] belongs to the class of gauge inflation models [45–47]. The main motivation of these models is to generate a sufficiently flat inflaton potential protected by gauge symmetries because the inflaton field is part of a

gauge field. As a consequence, it is safe to consider super-Planckian values for the inflaton field. Because its potential is similar to the (smooth) hybrid one, this model is also interesting to determine how generic the properties of initial conditions observed for other models are, for different types of models, originating from different high energy frameworks.

2. The potential

In the simplest version of these models, an effective five-dimensional universe is assumed, one of the dimension being compactified with a radius[8] R. In the gauge inflation model, a gauge symmetry is assumed together with a gauge field (A_μ, A_5). The inflaton field is proportional to the phase θ of a Wilson-loop wrapped around the compact dimension $\theta = \oint dx^5 A_5$. The full inflaton field is constructed with the symmetry breaking scale f of the gauge symmetry $\phi \equiv f\theta$. Its potential is flat at tree level but at one-loop, takes the form of an axionlike potential

$$V(\phi) \propto \frac{1}{R^4}\cos(\phi/f). \tag{35}$$

The potential is protected from nonrenormalizable operators, suppressed by powers of $1/R$, while nonperturbative quantum gravity corrections can be suppressed [46,47]. Another motivation concerns the initial homogeneity of the inflaton field, necessary for inflation to start. Finally, since the inflaton is a phase, one can show [44] that the probability to have a sufficiently homogeneous distribution of the field is quite large.

The ''radion assisted'' gauge inflation differs from standard gauge inflation by assuming a varying radius of the extra-dimension R, around a central value R_0. The ''radion'' field is defined by[9] $\psi \equiv (2\pi R)^{-1}$ and is subject to a potential for which R_0 is assumed to be the minimum (for the late time stability of the extra-dimension). The simplest way to implement this stabilization is to use a Higgs-type potential for ψ. By expanding, at first order, the potential of Eq. (35), and by adding the Higgs-type sector, the full scalar potential reads [24]

$$V(\phi, \psi) = \frac{1}{4}\frac{\phi^2}{f^2}\psi^4 + \frac{\lambda}{4}(\psi^2 - \psi_0^2)^2, \tag{36}$$

where $\psi_0 = (2\pi R_0)^{-1}$. This potential is similar to the hybrid potential discussed in the last section. It is flat for $\psi = 0$ which corresponds to a global maxima. For a given ϕ, the minima of the potential are located in the valleys

$$\langle\psi\rangle^2 = \frac{\psi_0^2}{1 + \phi^2/(\lambda f^2)}. \tag{37}$$

More than 60 e-folds of inflation can take place in these throats.

3. Space of initial conditions

Regarding the allowed parameter space that can be studied, since ψ is the inverse of the radius of an extra-dimension and quantum gravity effects are expected to dominate when the field gets larger than the five dimensional Planck mass. Thus super-Planckian values of ψ or ψ_0 should not be taken into account if one does not consider the potential of Eq. (36) as an effective model. For the first set of values of the parameters ($\psi_0 = 10^{-2} m_{\rm pl}$, $f = m_{\rm pl}$, $\lambda = 10^{-5}$), the grid of initial conditions is very similar to the hybrid case, with a triangular unsuccessful region, and a generic successful inflation at larger values of the fields (see Fig. 13 below).

Many successful trajectories also appear in the unsuccessful area (type-C trajectories), for sufficiently small values of λ. We observe a slightly higher successful area, compared to the hybrid case: for $\phi_{\rm i}$, $\psi_{\rm i} < M_{\rm pl}$, more than 20% of the points are successful. Grids for different values of the parameter M show a behavior similar to the hybrid model. However, varying λ has a major impact on the amount of type-C trajectories as shown in Table II. In particular we do not find a significant amount of successful initial conditions for the choice of parameters of [24]

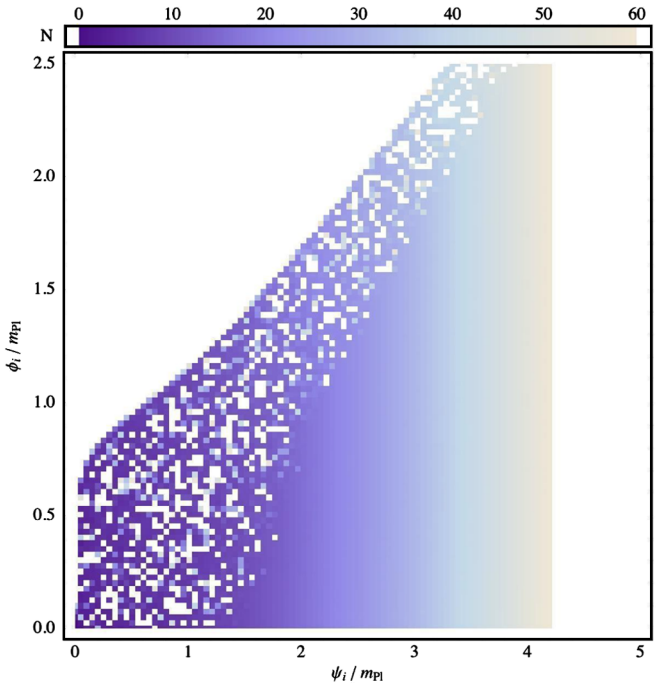

FIG. 13 (color online). Grid of initial conditions for radion potential, with $\psi_0 = 10^{-2} m_{\rm pl}$, $f = 1 m_{\rm pl}$, $\lambda = 10^{-5}$.

[8]The effective four-dimensional (reduced) Planck mass is related to the five-dimension Planck mass M_5 by $M_{\rm pl}^2 = 2\pi R M_5^3$.

[9]In our simulations below, we allowed the ψ field to take negative values because the symmetries of the potential allow to redefine the field as $|\psi| \equiv (2\pi R)^{-1}$, so that the length of the extra-dimension stays positive.

TABLE III. Percentage of successful points in grids of initial conditions of length $5m_{\rm pl}$, for each model and some standard values of the parameters.

Model	Values of parameters	Successful (%)
Hybrid	$M = 0.03$, $m = 10^{-6}$, $\lambda = \lambda' = 1$	72
Smooth	$M \approx 2.37 \times 10^{-5} m_{\rm pl}$, $\kappa \approx 10.3$	92
Shifted	$M = 10^{-2} m_{\rm pl}$, $\kappa^2 = 1$, $\beta = 10^{-2} m_{\rm pl}^{-2}$	73
Radion	$\psi_0 = 10^{-2} m_{\rm pl}$, $\lambda = 10^{-3}$, $f = 1$	76

($\psi_0 = 10^{-2} m_{\rm pl}$, $f = 1 m_{\rm pl}$, $\lambda = 10^{-3}$). We also observe a transition between the successful and unsuccessful region less abrupt (see Fig. 13). This is due to the fact that at small inflaton field, the potential slightly differs from the hybrid potential: the slope of the potential is slightly more steep and the same amount of e-folds requires a larger variation of field values.

Our results on the proportion of successful initial conditions for all models are summarized in the Table II below, when restricting to initial fields values below the reduced Planck mass. For comparison the results for the original hybrid model are recalled. Two percentages are given: first the total number of successful initial field values (column 3) and the number of initial conditions that are scattered in the initial condition space, outside of the inflationary valley(s) (column 4). For these cases, the realization of inflation is called in this paper anamorphosis: the system fast-rolls down the potential, oscillates around the bottom of the potential, climbs up one of the valleys and slow-rolls down along it as if it started in the valley. When relevant, the number of the figure representing the space of initial field values is given in column 5.

From the different grids of initial values for the various models studied in this paper, it is obvious that if we do not require that the fields are smaller than the reduced Planck mass, the proportion of successful initial conditions will tend toward 100% except when considering models in SUGRA. Therefore, we have also conducted the same quantification with the requirement $\phi_i,\ \psi_i < 5m_{\rm pl}$. The results are given in Table III below. This quantification has been computed only to give an information about how fast the proportion of successful initial conditions increases when the space of allowed initial values is enlarged.

IV. CONCLUSIONS

Hybrid inflation is a class of models of inflation motivated by high energy physics. In these models, the inflaton field is assumed to be coupled to a Higgs-type auxiliary field that ends inflation by instability, when developing a nonvanishing expectation value. Two of its main well-known problems—the blue spectrum of the nonsupersymmetric version of the model and the fine-tuning of the initial conditions of the fields—are reanalyzed.

First, we found that the original hybrid model can generate a red spectrum by two means. As well-known, one way to have inflation takes place in the large field phase is to have the waterfall ending inflation in that phase. This requires a constraint on the critical value of the inflaton triggering the waterfall. We found a new criteria on the mass scale μ so that a violation of the slow-roll conditions ensures the *nonexistence of the small field phase of inflation*. In both cases, the spectral index generated is less than unity (see Fig. 3). However, we show that this requires in both cases a large initial value of the inflaton ($> m_{\rm pl}$), and therefore a realization of hybrid inflation in a regime away from the limit $\phi \ll \mu$. This conclusion might reduce the appeal of this model.

When considering the full two-field potential, it was found [29–31] that the original models suffer from a fine-tuning of the initial values of the fields to generate a sufficiently long inflationary phase. The space of successful inflation was thought to be composed of a extremely narrow band along the inflationary valley and some ''isolated scattered points'' which seemed randomly distributed and of null measure [31]. It was therefore considered that these models suffered from some naturalness problem.

We have numerically integrated the exact equations of motion of both fields and studied in details the space of initial conditions. The study has been conducted for four different models of hybrid-type inflation in various frameworks: the original nonsupersymmetric model (Sec. II), its extensions smooth and shifted hybrid inflation in global supersymmetry and supergravity and the ''radion assisted'' gauge inflation (Sec. III). As expected, we found that for sufficiently large initial values of the fields (Planckian-like or super-Planckian), enough e-folds of inflation are generated (see for e.g. Fig. 4). This behavior is similar to the one of chaotic inflation [61]. We also studied the shape of the unsuccessful region and its dependence on the potential parameters: this property holds for any values of the parameters and all the models we considered, except when embedded in supergravity. Consequently, the first way to solve the fine-tuning problem of initial conditions for hybrid models is to formulate them in a framework for which it is safe to consider Planckian-like or super-Planckian initial values for the fields. This can be safe or problematic, depending on the framework used to build the model as detailed in the introduction.

Even if the considered model is formulated in a framework where the fields cannot safely be super-Planckian, the unsuccessful region of initial conditions contains successful subregions. They correspond to special trajectories for which the velocity in field space becomes oriented along the inflationary valley after some oscillations at the bottom of the potential. Therefore the system climbs up the valley before slow-rolling back down, generating enough inflation. We find that these points form a complex structure, as represented in Fig. 7. They can be seen as the anamorphosis

of the standard inflationary valley, and explain most of the successful initial conditions when restricting to sub-Planckian fields. The relative area that these points occupy is typically of order of 15% for the original hybrid model. This value can go up to 25% for radion inflation and even above 70% for smooth inflation, even though these results depend on the values of the parameters of the potential (see Table II). Moreover, even when supergravity corrections are included, these trajectories still exist, their proportion stays similar and they represent even more of the successful initial conditions. We would like to note that these percentages allow us to claim that the fine-tuning on hybrid inflation is less severe that found in the past. However, to translate this into an amount of fine-tuning for the model, it is necessary to compute a measure of the probability space. This is left for an extension of this work [67].

Several other questions remain open and are extensions of this work. We plan on investigating more deeply the statistical properties of the anamorphosis regions of the plane of initial conditions as well as the effects of initial velocities on this plane [68]. The study of the supersymmetric versions of hybrid inflation, the F-term [17] and D-term [15,16] models are also left for a future study. These models could have a different dynamics from the models studied here since radiative corrections generate potentially important corrections to the tree level potential [69].

Finally, our results illustrated that the successful realizations of hybrid inflation are not necessarily by fast-roll toward the inflationary valley as usually assumed but also radially (type-B trajectories), and in that sense chaoticlike. Some aspects of the phenomenology of these purely two-field trajectories (power spectrum, generation of non-Gaussianities, stochastic effects, reheating, impact on topological defect formation) are still unknown and should be studied.

ACKNOWLEDGMENTS

It is a pleasure to thank J. Martin, C. Ringeval, and M. Tytgat for many interesting discussions and a careful reading of the manuscript. J. Garcia-Bellido and L. McAllister are also acknowledged for useful comments. S. C. is supported by the Belgian Fund for research (F.R.I.A.). J. R. is funded in part by IISN and Belgian Science Policy IAP VI/11.

[1] Alexei A. Starobinsky, Phys. Lett. B **91**, 99 (1980).
[2] Alan H. Guth, Phys. Rev. D **23**, 347 (1981).
[3] Andrei D. Linde, Phys. Lett. B **108**, 389 (1982).
[4] Andrei D. Linde, Particle Physics and Inflationary Cosmology, 2005.
[5] *Inflationary Cosmology*, edited by M. Lemoine, J. Martin, and P. Peter, Lect. Notes Phys. Vol. 738 (Springer, Heidelberg, 2008).
[6] Robert H. Brandenberger, Ali Nayeri, Subodh P. Patil, and Cumrun Vafa, Int. J. Mod. Phys. A **22**, 3621 (2007).
[7] Patrick Peter, Emanuel J. C. Pinho, and Nelson Pinto-Neto, Phys. Rev. D **75**, 023516 (2007).
[8] Patrick Peter and Nelson Pinto-Neto, Phys. Rev. D **78**, 063506 (2008).
[9] David H. Lyth and Antonio Riotto, Phys. Rep. **314**, 1 (1999).
[10] Andrei Linde, econf C040802, L024 (2004).
[11] Renata Kallosh, Lect. Notes Phys. **738**, 119 (2008).
[12] E. Komatsu *et al.*, Astrophys. J. Suppl. Ser. **180**, 330 (2009).
[13] Andrei D. Linde, Phys. Rev. D **49**, 748 (1994).
[14] Edmund J. Copeland, Andrew R. Liddle, David H. Lyth, Ewan D. Stewart, and David Wands, Phys. Rev. D **49**, 6410 (1994).
[15] Edi Halyo, Phys. Lett. B **387**, 43 (1996).
[16] P. Binétruy and G. R. Dvali, Phys. Lett. B **388**, 241 (1996).
[17] G. R. Dvali, Q. Shafi, and Robert K. Schaefer, Phys. Rev. Lett. **73**, 1886 (1994).
[18] Renata Kallosh and Andrei Linde, J. Cosmol. Astropart. Phys. 10 (2003) 008.
[19] R. Jeannerot, Phys. Rev. D **56**, 6205 (1997).
[20] Rachel Jeannerot, Jonathan Rocher, and Mairi Sakellariadou, Phys. Rev. D **68**, 103514 (2003).
[21] G. R. Dvali and S. H. Henry Tye, Phys. Lett. B **450**, 72 (1999).
[22] Fumikazu Koyama, Yuji Tachikawa, and Taizan Watari, Phys. Rev. D **69**, 106001 (2004).
[23] Takeshi Fukuyama, Nobuchika Okada, and Toshiyuki Osaka, J. Cosmol. Astropart. Phys. 09 (2008) 024.
[24] M. Fairbairn, Laura Lopez Honorez, and M. H. G. Tytgat, Phys. Rev. D **67**, 101302 (2003).
[25] Dalia S. Goldwirth and Tsvi Piran, Phys. Rep. **214**, 223 (1992).
[26] Tanmay Vachaspati and Mark Trodden, Phys. Rev. D **61**, 023502 (1999).
[27] Nemanja Kaloper, Matthew Kleban, Albion Lawrence, Stephen Shenker, and Leonard Susskind, J. High Energy Phys. 11 (2002) 037.
[28] Andrei D. Linde, Phys. Lett. B **175**, 395 (1986).
[29] N. Tetradis, Phys. Rev. D **57**, 5997 (1998).
[30] George Lazarides and N. D. Vlachos, Phys. Rev. D **56**, 4562 (1997).
[31] Luis E. Mendes and Andrew R. Liddle, Phys. Rev. D **62**, 103511 (2000).
[32] George Lazarides, C. Panagiotakopoulos, and N. D. Vlachos, Phys. Rev. D **54**, 1369 (1996).
[33] Esteban Calzetta and Maria Sakellariadou, Phys. Rev. D **47**, 3184 (1993).
[34] S. Dimopoulos, S. Kachru, J. McGreevy, and Jay G. Wacker, N-flation, 2005.

[35] Richard Easther and Liam McAllister, J. Cosmol. Astropart. Phys. 05 (2006) 018.
[36] Bret Underwood, Phys. Rev. D **78**, 023509 (2008).
[37] Rudnei O. Ramos, Phys. Rev. D **64**, 123510 (2001).
[38] C. Panagiotakopoulos and N. Tetradis, Phys. Rev. D **59**, 083502 (1999).
[39] George Lazarides and C. Panagiotakopoulos, Phys. Rev. D **52**, R559 (1995).
[40] George Lazarides and Achilleas Vamvasakis, Phys. Rev. D **76**, 083507 (2007).
[41] Masahide Yamaguchi and Jun'ichi Yokoyama, Phys. Rev. D **70**, 023513 (2004).
[42] R. Jeannerot, S. Khalil, George Lazarides, and Q. Shafi, J. High Energy Phys. 10 (2000) 012.
[43] R. Jeannerot, S. Khalil, and George Lazarides, J. High Energy Phys. 07 (2002) 069.
[44] Katherine Freese, Joshua A. Frieman, and Angela V. Olinto, Phys. Rev. Lett. **65**, 3233 (1990).
[45] Nima Arkani-Hamed, Hsin-Chia Cheng, Paolo Creminelli, and Lisa Randall, Phys. Rev. Lett. **90**, 221302 (2003).
[46] Nima Arkani-Hamed, Hsin-Chia Cheng, Paolo Creminelli, and Lisa Randall, J. Cosmol. Astropart. Phys. 07 (2003) 003.
[47] David E. Kaplan and Neal J. Weiner, J. Cosmol. Astropart. Phys. 02 (2004) 005.
[48] Daniel Baumann and Liam McAllister, Advances in Inflation in String Theory, 2009.
[49] Jonathan P. Hsu, Renata Kallosh, and Sergey Prokushkin, J. Cosmol. Astropart. Phys. 12 (2003) 009.
[50] S. H. Henry Tye, Lect. Notes Phys. **737**, 949 (2008).
[51] Eva Silverstein and Alexander Westphal, Phys. Rev. D **78**, 106003 (2008).
[52] Dominik J. Schwarz, Cesar A. Terrero-Escalante, and Alberto A. Garcia, Phys. Lett. B **517**, 243 (2001).
[53] Dominik J. Schwarz and Cesar A. Terrero-Escalante, J. Cosmol. Astropart. Phys. 08 (2004) 003.
[54] Jerome Martin and Christophe Ringeval, J. Cosmol. Astropart. Phys. 08 (2006) 009.
[55] Jerome Martin, Braz. J. Phys. **34**, 1307 (2004).
[56] Antonio Cardoso, Phys. Rev. D **75**, 027302 (2007).
[57] Andrei D. Linde, Dmitri A. Linde, and Arthur Mezhlumian, Phys. Rev. D **49**, 1783 (1994).
[58] Jerome Martin and Marcello Musso, Phys. Rev. D **73**, 043516 (2006).
[59] Andrew R. Liddle and Samuel M. Leach, Phys. Rev. D **68**, 103503 (2003).
[60] Christophe Ringeval, Lect. Notes Phys. **738**, 243 (2008).
[61] Andrei D. Linde, Phys. Lett. B **129**, 177 (1983).
[62] Jonathan Rocher and Mairi Sakellariadou, J. Cosmol. Astropart. Phys. 03 (2005) 004.
[63] Rachel Jeannerot and Marieke Postma, J. High Energy Phys. 05 (2005) 071.
[64] Aurelien A. Fraisse, J. Cosmol. Astropart. Phys. 03 (2007) 008.
[65] Neil Bevis, Mark Hindmarsh, Martin Kunz, and Jon Urrestilla, Phys. Rev. Lett. **100**, 021301 (2008).
[66] A. Vilenkin and P. Shellard, *Cosmic Strings and Other Topological Defects. 1994*, Cambridge monographs on mathematical physics (Cambridge University Press, Cambridge, England, 1994).
[67] Sébastien Clesse, Christophe Ringeval, and Jonathan Rocher (unpublished).
[68] Sébastien Clesse and Jonathan Rocher (unpublished).
[69] Bart Clauwens and Rachel Jeannerot, J. Cosmol. Astropart. Phys. 03 (2008) 016.